Lin *et al. Microstructures* 2024;4:2024053
DOI: 10.20517/microstructures.2024.30

Microstructures

Research Article

Open Access

Check for updates

Sandwich-structured electrospun polyvinylidene difluoride sensor for structural health monitoring of glass fiber reinforced polymer composites

Haokun Lin[1], Yunsong Peng[2], Fengjia Zhang[1], Xucheng Ke[3], Liman Sai[3], Feifei Wang[3], Helezi Zhou[1], Nan Zheng[4], Zhigao Huang[1], Huamin Zhou[1]

[1]State Key Laboratory of Materials Processing and Die & Mould Technology, School of Materials Science and Engineering, Huazhong University of Science and Technology, Wuhan 430074, Hubei, China.
[2]Luoyang Ship Material Research Institute, Luoyang 471000, Henan, China.
[3]Key Laboratory of Optoelectronic Materials and Device, Department of Physics, Shanghai Normal University, Shanghai 200234, China.
[4]School of Light Industry and Chemical Engineering, Dalian Polytechnic University, Dalian 116034, Liaoning, China.

Correspondence to: Assoc. Prof. Helezi Zhou, State Key Laboratory of Materials Processing and Die & Mould Technology, School of Materials Science and Engineering, Huazhong University of Science and Technology, 1037, Luoyu Road, Hongshan District, Wuhan 430074, Hubei, China. E-mail: helezizhou@hust.edu.cn

How to cite this article: Lin H, Peng Y, Zhang F, Ke X, Sai L, Wang F, Zhou H, Zheng N, Huang Z, Zhou H. Sandwich-structured electrospun polyvinylidene difluoride sensor for structural health monitoring of glass fiber reinforced polymer composites. *Microstructures* 2024;4:2024053. https://dx.doi.org/10.20517/microstructures.2024.30

Received: 27 Mar 2024 **First Decision:** 12 Jun 2024 **Revised:** 30 Jun 2024 **Accepted:** 5 Jul 2024 **Published:** 2 Sep 2024

Academic Editors: Shujun Zhang, Andrea Sanson **Copy Editor:** Fangling Lan **Production Editor:** Fangling Lan

Abstract

Stress monitoring and interlaminar failure detection attract much attention in glass fiber reinforced polymer (GFRP) structural health monitoring area. However, due to limitations of sensing or electrode materials, existing embedding sensors cannot be designed to have both of the abilities without sacrificing mechanical properties. This work fabricated a sandwich-structured sensor, which is composed of three layers of electrospun polyvinylidene difluoride membranes. The upper and lower electrodes are flexible membranes that ensure stable signal collection in the rigid GFRP material system. The sensor can quantitatively monitor the stress based on piezoelectric effect, and interlaminar crack propagation based on parallel plate capacitors. The voltage and capacitance values have a linear relationship with the stress level and crack length (R-square of the functions is 0.999 and 0.933), respectively. Due to the porous microstructure of electrospun membranes, polymer matric can well infiltrate the polyvinylidene difluoride nanofibers while preparing the sensor embedded GFRP. Thus, the perfect bonding of the sensor within GFRP ensures the effective sensing abilities until sample failure and negligible effect (< -7%) on the mechanical properties of GFRP.

Keywords: Glass fiber reinforced polymer composites, electrospun PVDF, sandwich-structured sensor, stress monitoring, interlaminar crack monitoring

INTRODUCTION

Glass fiber reinforced polymers (GFRP) possess corrosion-resistant properties and excellent mechanical abilities[1,2], thereby making them a prevalent material in marine and aerospace equipment[3]. However, the inevitable damage accumulation may lead to the failure of GFRP components and consequential financial losses. So, *in situ* stress and damage monitoring of GFRP is important[4,5]. In particular, interlaminar crack is considered to be the most dangerous in laminate composite structures[6-8].

Currently, many technologies have been made in monitoring the stress and strain of GFRP during service[9], such as strain gauges[10], fiber optic sensors[11-13], piezoelectric sensors[14] and piezoresistive sensors[15]. If the sensors are bonded to the surface of the component, they may debond due to impact or long-term service. Thus, embedded sensors are a better alternative[16]. However, since the existing embedded sensors (such as optical fibers[13] and ceramic piezoelectric sensors[17]) are thicker than the interlayer of the laminate or have weak interfacial bonding with the polymer matrix, they may cause severe mechanical effects[18] on the carbon fiber reinforced polymer (CFRP) composites. To minimize the effect on mechanical performances, our group[19] has designed an embedded sensor based on the commercial piezoelectric polyvinylidene difluoride (PVDF) film. The sensor can achieve stress monitoring without sacrificing static and fatigue mechanical performances of the fiber composites. However, the interlaminar crack detection was not realized. Piezoresistive nanocomposite sensors are also an upcoming choice[16]. Wang *et al.* designed a piezoresistive nanocomposite sensor for structural health monitoring (SHM)[20]. This sensor causes negligible mechanical impact on composites, but it is only applied to the new GFRP structure type presented in their work and it cannot monitor interlaminar cracks either.

Several works have developed interlaminar crack monitoring methods depending on electrical conductivity of the laminate. The researchers used a variety of approaches, such as buckypapers[21,22], graphene[23], carbon nanotubes (CNTs)[24,25] and carbon black[26], to monitor interlaminar crack propagation in CFRP. For insulation fabric-based composites such as GFRP, it is necessary to improve the interlaminar conductivity to achieve interlaminar crack monitoring[27]. For example, Wu *et al.* incorporated conductive nanofillers into the epoxy resin of GFRP to improve its conductivity, thus enabling GFRP to detect interlaminar crack development[8]. Kravchenko *et al.* introduced conductive interlaminar interfaces into GFRP, and achieved interlaminar crack monitoring[28]. In summary, such methods necessitate external power supply and the composites must be conductive in the crack propagation sensing.

Except the above-mentioned sensing materials, nanofiber membranes showed outstanding sensing performances, such as used for dielectric capacitors[29], electronic skins[30], glucose sensors[31], wearable pressure sensors[32], flexible thermoelectric generators[33] and gas sensors[34]. For GFRP composites, the porous structure of nanofiber membranes facilitates polymer matrix infiltration and good interfacial bonding inside the composites[35]. This makes nanofiber membranes a good choice as a material for embedded sensors in GFRP. Cheng *et al.* use electrospun PVDF as sensing material and make carbon fiber as electrodes to get damage signal[36]. However, it can only identify the occurrence of damage but not quantify the damage. The sensing abilities of the nanofiber membranes in composites can be further explored.

In summary, one of the critical challenges of sensors is that they cannot realize both stress monitoring and interlaminar crack monitoring. Another is that the integrated sensors may degrade the mechanical properties of composites. In this work, we designed a sandwich-structured PVDF nanofiber sensor for

GFRP monitoring without sacrificing mechanical performances. It is capable of monitoring both stress and interlaminar crack propagation. The piezoelectric voltage signal of sensors shows remarkable linearity with applied force. For interlaminar cracks, we conducted *in-situ* monitoring by capturing capacitance signals. Various mechanical tests are conducted to analyze the effect of the sensor on the tensile, bending, and interlaminar shear and fracture toughness.

MATERIALS AND METHODS

Preparation of sensors

The PVDF fiber membrane is prepared by electrospinning. We mix the N,N-Dimethylformamide (DMF, Sinopharm Chemical Reagent Corporation, Shanghai, China) and acetone at a solvent weight ratio of 3:2 to prepare a solution. Then, the raw PVDF powder is dissolved in the solution at a powder/solvent weight ratio of 1:9. The PVDF solution is used for electrospinning. The applied voltage is 20 kV, the propulsion speed (flow rate) is 1.5 mL/h, the collection roller speed is 25 rpm, the spacing between the needle tip and collector is 20.5 cm, and the amount of spinning solution is about 25 mL. The as-spun nanofibers are collected on the aluminum foil and dried at 80 °C for 4 h. The Scanning Electron Microscope (SEM) image shows the electrospun PVDF [Figure 1]. The fiber diameter is uniform and there is no agglomeration, adhesion or other phenomena. PVDF nanofibers have smooth surfaces and the diameter of single fibers is found at a similar size of ~500 nm, the same as our previous work[37].

Using piezoresponse force microscopy (PFM), the piezoelectric response of a single PVDF nanofiber is characterized. Figure 2 shows the measured topography (a), amplitude (b), and phase (c) images of a single PVDF nanofiber under an alternating current (AC) voltage of 1.5 V and 60 V direct current (DC) bias in a $10 \times 10\ \mu m^2$ area. The microscopic amplitude and phase of single PVDF nanofibers shown in Figure 2B and C manifested the presence of local ferroelectric domains with clear ferroelectric polarization. The bright and dark contrast in Figure 2C further indicates the presence of different polarized neighboring domains. The local piezoelectric responses of three randomly selected points 1, 2, and 3 in Figure 2A were recorded and shown in Figure 2D-F. The phases of these three points flip with the direction of the electric field, which is due to the existence of domains inside the PVDF nanofiber. The displacement-voltage curves of all three points show the typical butterfly-shaped loop, indicating the strong piezoelectricity on single PVDF nanofiber. This also shows that electrospun PVDF is suitable as a sensing material in GFRP.

The PVDF fiber membrane serves as the piezoelectric material and capacitor medium. Since the electrodes are difficult to integrate onto the porous structure of PVDF membrane as in our previous work[19], suitable electrodes are indispensable. The electrodes are utilized as piezoelectric signal collectors or capacitor parallel plates in multiple sensing conditions, as shown in Figure 3A. The principle of sandwich-structured sensor severs as piezoelectric and capacitive sensors is also explained. When the sandwich-structured PVDF sensor is subjected to external force, the PVDF as piezoelectric material is stretched and generates electrical charges. The porous media electrodes as piezoelectric signal collectors collect and output voltage signals. When the crack destroys PVDF as dielectric material, the dielectric between porous media electrodes as parallel plates decreases and the capacitance drops.

Porous materials are selected as electrodes to diminish the mechanical impact on GFRP, as they can be infiltrated by resin. Thus, we preliminary choose two different electrode porous materials, Au-PVDF and CNT film. Au-PVDF film is prepared by Au deposition onto the surface of the electrospun PVDF fiber membrane by evaporation. PVDF is clamped on a special fixture of vacuum coating equipment (Chengdu vacuum machinery factory). The vacuum degree and temperature are around 1.0×10^{-3} Pa and 80 °C. Cr/Au was deposited as the first and second layers with 20 and 200 nm thicknesses, respectively. CNT film is

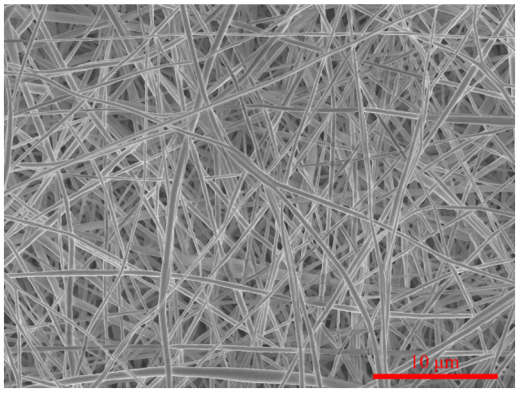

Figure 1. SEM image of electrospun PVDF.

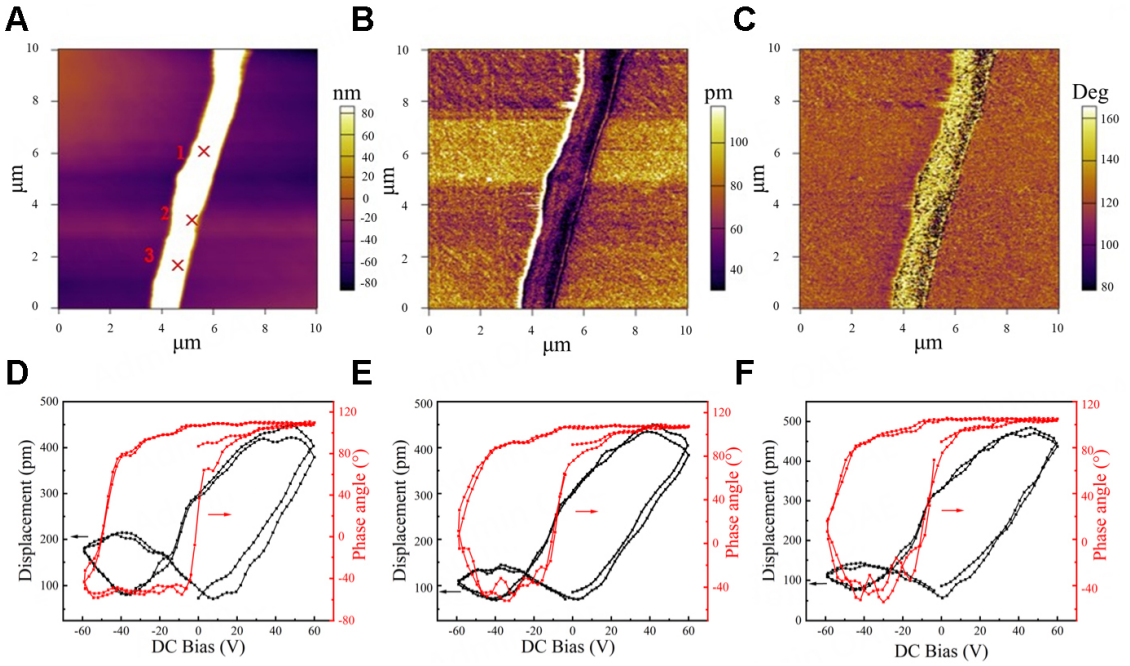

Figure 2. PFM images and local piezoelectric response of the PVDF nanofibers. (A-C) Height, amplitude, and phase of the PFM measurement of a single PVDF nanofiber; (D-F) local field-induced displacement curve corresponding to points 1, 2 and 3 in (A).

purchased from TIMESNANO. A copper electrode is commonly used for a flexible sensor; it is also tried in our experiments for comparison.

GFRP fabrication

GFRP laminates were produced by vacuum-assisted resin infusion (VARI). The woven glass fabric EWR200 from Changzhou Zhongjie Composite Materials Co., Ltd was used with an area density of 200 g/m^2. The GFRP matrix is Huntsman Araldite LY 1564 resin and Aradur 22962 epoxy curing agent from Huntsman Advanced Materials, with a mixed weight ratio of 4:1. The sample was cured at 78 °C for 8 h.

Sensors monitoring effect tests

Stress and strain monitoring

As shown in Figure 3B, piezoelectric signals were obtained by implanting the sensor into GFRP in a three-

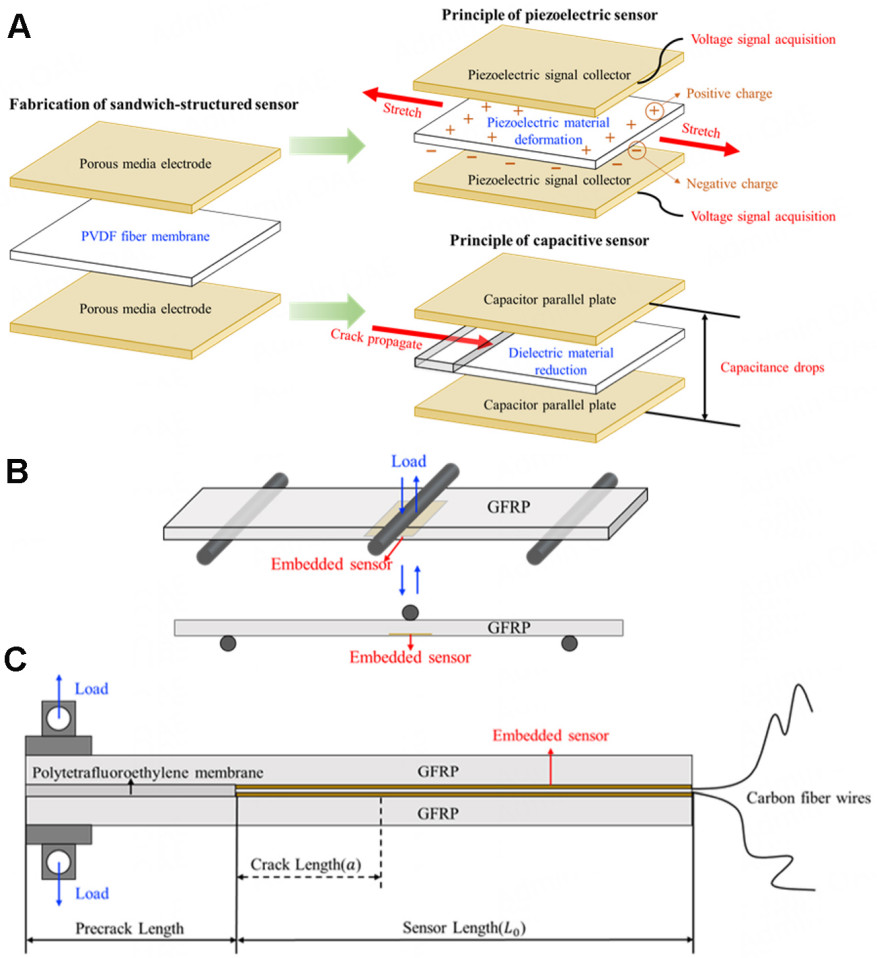

Figure 3. (A) Fabrication of sandwich-structured sensor, and the working principle of piezoelectric sensor and capacitive sensor; (B) GFRP with sandwich-structured sensor embedded test through dynamic three-point bending test; (C) GFRP with sandwich-structured PVDF embedded sensor in DCB test.

point bending test. The dynamic three-point bending test refers to ASTM D7264. The sample size is 100 mm × 15 mm × 3.5 mm, and the sensor size is 10 mm × 10 mm. The sensor is embedded between the lowest and penultimate layers of fabrics, and it is mainly subjected to tensile stress during the test. The voltage signal was acquired by data acquisition equipment (VK107H, Vkinging Co. Ltd., China). The charge generated must be converted to a voltage output by a charge amplifier. The output voltage V_{out} (mV) of the sandwich sensor was imported into the LabView program and calculated using:

$$V_{out} = QG_{ain}K_c \tag{1}$$

where Q indicates the amount of charge generated by PVDF, G_{ain} denotes the magnification of charge amplifier (G_{ain} =4), and K_c represents the charge amplification sensitivity (K_c = 1 pC/mV).

Interlaminar crack monitoring

As shown in Figure 3C, The sandwich-structured sensor forms a parallel plate capacitor. Based on the double cantilever beam (DCB) test, the sensor is embedded in the test area of the interlaminar fracture test sample. And the polytetrafluoroethylene membrane is used as a pre-crack. The mode I interlaminar fracture

toughness test is preformed according to ASTM D5528 test standard, the sample size is 200 mm × 22 mm × 3.5 mm, the sensor size is 20 mm × 50 mm, and the pre-crack length is 60 mm. The capacitance signal is collected by the data acquisition equipment (LCR-8000G, Good Will Instrument Co., Ltd, Taiwan). The output capacitance C_{out} (pF) follows the capacitance formula for a parallel plate capacitor:

$$C_{out} = \frac{\varepsilon_2 A_{Au-PVDF}}{d} \times \frac{L_0 - a}{L_0} \tag{2}$$

where ε_2 is dielectric constant of PVDF infiltrated by epoxy resin, $A_{Au\text{-}PVDF}$ is the area of Au-PVDF (mm^2), d is the thickness of PVDF (mm), L_0 is the length of sensor (mm), and α is the crack length (mm). While the crack propagates (α increases), the dielectric in the middle layer of the parallel plate capacitor is damaged, the relative area is reduced, and the capacitance C_{out} will decline.

Mechanical performance tests

Through tensile tests, three-point bending and short beam shear (SBS), the effect of sandwich-structured PVDF sensors on the mechanical properties of GFRP is explored. The tensile test of GFRP is carried out according to ASTM D3093. The sample size is 250 mm × 25 mm × 2.5 mm. The sensor is embedded in the middle of the sample, and its size is 20 mm × 20 mm. The tensile test instrument is a general testing system (Shimadzu® AG-IC 100 kN), with a loading speed of 2 mm/min until the sample breaks. The tensile strength σ_t (Mpa) can be calculated by:

$$\sigma_t = \frac{P^{max}}{b \times h} \tag{3}$$

where P^{max} is the maximum force before failure (N), and b and h are the width and thickness of the specimen (mm).

The three-point bending test is conducted on the general test system (Zwick® Z020) according to the ASTM D7264 test standard. The size of the sample is 100 mm × 15 mm × 3.5 mm. The sensor is embedded between the lowest layer and the penultimate layer of fabric. The size of the implanted sensor is 15 mm × 15 mm. The loading head speed is 1.5 mm/min, the span-to-thickness ratio is 16:1, and at least five samples are tested in each group. The flexural strength σ_f (MPa) can be calculated by:

$$\sigma_f = \frac{3PL}{2bh^2} \tag{4}$$

where P is the maximum load (N), L is the support span (mm), and b and h are the width and thickness of the specimen (mm).

The SBS test is tested on a general test system (Zwick® Z020) according to the ASTM D2344 test standard. The sample size is 21 mm × 7 mm × 3.5 mm. The sensor is embedded in the middle of the sample, and the size of the embedded sensor is 10 mm × 7 mm. Loading head speed was 1 mm/min. The span-to-thickness ratio is 4:1. The interlaminar shear strength (ILSS) τ_s (MPa) can be calculated by:

$$\tau_s = 0.75 \times \frac{P}{b \times h} \tag{5}$$

where P is the maximum load (N), and b and h are the width and thickness of the specimen (mm).

RESULTS AND DISCUSSION

Online monitoring tests

Choice of electrode material

GFRP specimens with copper, Au-PVDF and CNT film electrode sensors are tested under dynamic loading. As shown in Figure 4A, the copper electrode sensor embedded CFRP produces the highest signal peak, but the signal peaks are inconsistent. It is speculated that the modulus of the copper and the electrospun PVDF do not match, which affects the deformation of PVDF and the voltage signal. The CNT film electrode sensor one produces the lowest signal peak among the three sensors, and the signal peaks are inconsistent either. It is speculated that the high modulus CNT may pierce the PVDF fiber membrane, resulting in electrical conductivity between the two electrodes of the sensor.

The Au-PVDF electrode sensor embedded GFRP produces consistent signal peaks. The similar microstructure of the Au-PVDF and PVDF membranes ensures stable contact between the electrode and the middle sensing membrane during CFRP deformation; the close modulus of the nanofibers in Au-PVDF and PVDF membranes prevents the Au-PVDF nanofibers piercing the middle layer. These two points ensure that the sandwich-structured sensor can stably generate and collect piezoelectric signals. As a result, the Au-PVDF electrode is chosen as the electrode for the sensor in the following experiments.

The polished cross section of the Au-PVDF electrode sensor embedded GFRP after signal test is shown in Figure 4B. There is no delamination at the fabric layer/Au-PVDF interface (see red dotted lines in Figure 4B) and Au-PVDF/PVDF interface (see white dotted lines in Figure 4B), proving that the Au-PVDF electrode had good bonding with PVDF. In Figure 4B, there are observable resin-coated PVDF nanofibers in the PVDF layer. Upon examining the green dotted circle area in Figure 4B under higher magnification [Figure 4C], it is observed that the resin well penetrates the porous structure of the membrane and coats the PVDF nanofibers; thus, the Au-PVDF electrode sensor can *in-situ* monitor the stress/strain of GFRP.

Stress and strain monitoring

The stress and strain monitoring tests are conducted by dynamic three-point bending tests with a loading frequency of 2 Hz. The sandwich-structured PVDF sensor is embedded in the GFRP. The sensor experienced dynamic load during three-point bending tests. Testing was carried out for 100 cycles under several stress values (31, 62, 93, 124, 156, 187, 218 MPa).

The relationship between piezoelectric voltage signal and tensile stress is shown in Figure 5A. There is a linear relationship between the average maximum voltage signal V and the stress level σ (see the insert in Figure 5A). The linear relationship indicates the sandwich-structured PVDF sensor is appropriate to assess the stress of the sample.

The sensing ability was also evaluated in long service conditions by three-point bending fatigue test. As illustrated in Figure 5B, piezoelectric signals have been obtained over 50,000 cycles. The fatigue cycle can be divided into two stages (I/II). In stage I, the variations of the flexural strain and voltage peak signals were kept at 3.26% and 2.12%, which illustrated that the sensor has cyclic stability during service. The slight increment of the strain and signal is due to the decrease in stiffness of the specimen. In stage II, the voltage signals have several significant increments and slightly decreased, indicating the crack initiation and propagation inside the laminate. The sensor signal disappeared at the same time as the sample failed, which proved the durability of the sensor during service. Obviously, the voltage signals were more sensitive than

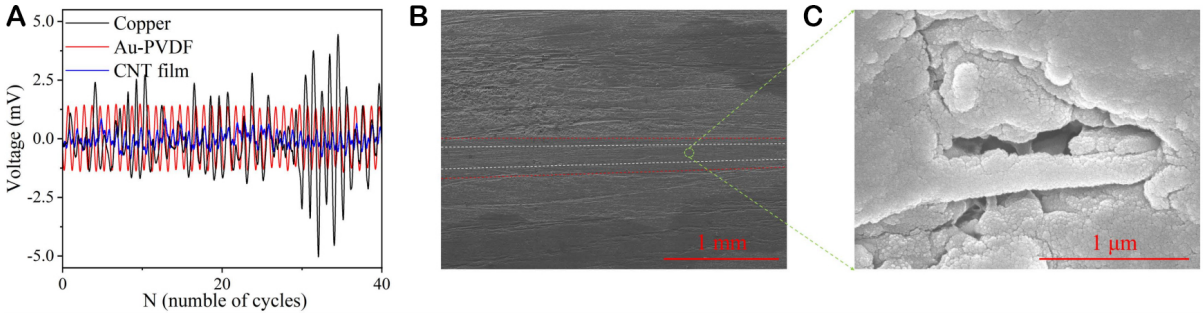

Figure 4. (A) Piezoelectric signals collected by copper electrode sensor, Au-PVDF electrode sensor and CNT film electrode sensor under dynamic three-point bending test within 40 cycles; SEM images of (B) the polished cross section of the Au-PVDF electrode sensor embedded GFRP; (C) Resin-coated PVDF nanofibers.

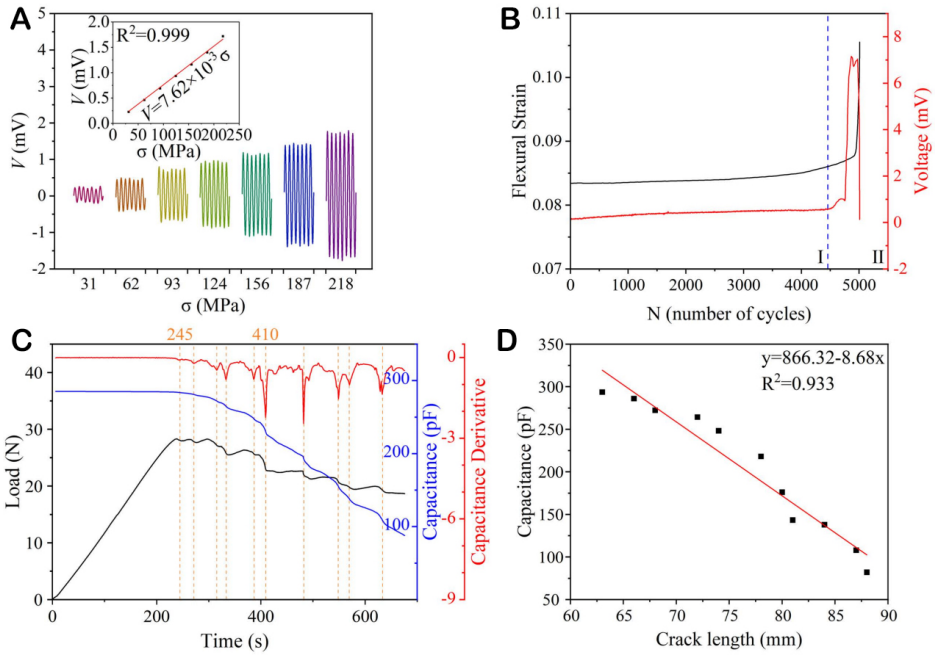

Figure 5. (A) Dependence of output voltage signal on different stresses. The inset shows the linear relationship between the piezoelectric signal and the stress on the sample; (B) Peak Voltage of the collected signals and flexural strain of the specimen during the three-point bending fatigue test; (C) Simultaneously recorded load and capacitance in DCB test, and the capacitance derivative *vs.* time curve; (D) The nearly linearly relationship between capacitance and the length of interlaminar crack in GFRP laminate.

the strain-cycle number curve, which increased gradually and then jumped suddenly at the end of stage II. Thus, this sensor can better reflect the interior damage in fatigue conditions than normal sensors, such as strain gauge sensors.

Interlaminar crack monitoring

The DCB test is used to investigate the initiation and propagation of interlaminar cracks in GFRP. To depict the initiation and propagation of cracks, the curves of the load, capacitance, and capacitance derivatives changing with time in the DCB test are presented in Figure 5C. As shown in Capacitance Derivative-Time and Load-Time curves, the first capacitance derivative decrease corresponds to the first load decrease. This indicates the sensor can pinpoint the crack initiation, thus accurately alerting the formation of the crack between layers. At 245 s, the initial crack propagation ends, as seen from the abrupt point in the Load-Time

curve and the curve's minimum point at 245 s in the Capacitance Derivative-Time curve.

According to the experimental criterion for mode I interlaminar fracture toughness, the point at which the Load-Time curve suddenly changes corresponds to the crack propagation. These points have a direct correspondence to the minimum value points of the Capacitance Derivative-Time curve. This phenomenon is analyzed based on the parallel plate capacitor principle of the sensor. For example, at 410 s in Figure 5C, the capacitance continues to decrease before the occurrence of crack propagation. The crack propagation results in a sudden decrease in capacitance and a minimum value point in capacitance derivative. Once the crack has completed its propagation, the capacitance stabilizes and tends towards 0 in terms of its derivative. The sudden changes in capacitance derivative correspond clearly to crack propagation and demonstrate the sensor's capability to monitor it, thereby aiding in the identification of composite failure. The relationship between capacitance and crack length is established, as illustrated in Figure 5D. As the crack propagates, capacitance shows a linear correlation with crack length.

As a summary, Table 1 lists some data from reported works related to the monitoring effect of composites with various integrated sensors. The sensor in this work realizes the monitoring of not only stress and failure of composite material components but also interlayer cracks of composites. Through horizontal comparison with other SHM sensors for composites, this work has achieved functional innovation.

Evaluation of mechanical performance

Basic mechanical properties

Figure 6A reflects the tensile test results of the experiment. The tensile strength of GFRP embedded with sensors decreased from 534.66 to 50 MPa (-5.16%), and the tensile modulus increased from 13.91 to 13.99 MPa (+0.61%). This indicates a slight decrease in tensile properties. Figure 6B demonstrates the reduction of flexural strength and flexural modulus in GFRP embedded with sensors, with the flexural strength declining from 499.43 to 486.62 MPa (-2.56%) and the flexural modulus declining from 20.44 to 19.15 GPa (-6.31%). The degradation of flexural properties is also relatively slight. The ILSSs are shown in Figure 6C. The sensors resulted in a decrease in the ILSS of GFRP from 38.04 to 36.74 MPa (-3.42%). It can be concluded that the sensors had little effect on the shear strength of GFRP. In summary, the composites embedded with sandwich-structured PVDF sensors showed a slight decrease (< 7%) in the basic mechanical properties. In our previous work[19], we summarized the mechanical effects of some embedded sensors (included in Table 2). In recent work, Han *et al.* used PVDF and barium titanate to monitor CFRP damage. When the content of PVDF and barium titanate increased, the flexural strength of CFRP decreased[51]. By summarizing these works [Table 2], the sensor in this work achieves relatively slighter mechanical performance degradation. The reason of this phenomenon requires further analysis through microscopic results.

Mode I interlaminar fracture toughness

The interlaminar fracture toughness was simultaneously investigated during the DCB test. As shown in Figure 6D and E, it was found that the interlaminar fracture toughness decreased. By implanting a single PVDF film as the GFRP interlayer, the effect of sensors on the fracture toughness of GFRP was further investigated. Mode I interlaminar fracture displacement-load curves are shown in Figure 6D. The comparison in Figure 6E shows that the PVDF sensor causes the G_{Ic}^{Ini} to decrease from 0.96 to 0.45 kJ/m^2 (-53.13%), while the single PVDF film can improve the G_{Ic}^{Ini} by 19.79% (1.15 kJ/m^2). For G_{Ic}^{Pro}, the PVDF sensor decreases it from 0.96 to 0.53 kJ/m^2 (-44.79%), and the single PVDF film improves it to 1.23 kJ/m^2 (+28.13%).

Table 1. Comparison of sensors monitoring effect in this work and other works

Material	Sensors	Variation in monitoring purpose			Remark	Reference
		Stress	Failure	Interlaminar crack		
GFRP	Sandwich electrospun PVDF	√	√	√	Linear relationship between voltage and stress Linear relationship between capacitance and interlaminar crack length (Δa)	This work
GFRP	Pt-PVDF film	√	√	\	\	[19]
CFRP	CNT and graphenes buckypaper	\	\	√	Relative resistance ($\Delta R/R_0$) + 12%	[21]
CFRP	Carbon nanostructure buckypaper	\	\	√	\	[22]
GFRP	Carbon nanostructure buckypaper	\	√	√	\	[28]
CFRP	ZnO NWs	√	√	\	Linear relationship between voltage and stress	[38]
CFRP	Graphene/epoxy interleave	\	\	√	$\Delta R/R_0$-Δa model developed	[23]
GFRP	Carbon nanofiber	\	\	√	$\Delta R/R_0$-Δa model developed	[39]
GFRP	CNT/polyvinyl alcohol film	√	√	\	\	[40]
GFRP	Graphene nanoplates (GNP)/epoxy pre-cured hybrid	√	\	\	Gauge factor = 26	[20]
GFRP	PES/carbon black Film	\	\	√	Sensitivity coefficient = 4.55	[26]
GFRP	CNT/epoxy mixture	\	√	\	Strain resolution = 0.01%	[41]
CFRP	CNT fabric coating	\	\	√	\	[24]
CFRP	CNT/GNP carbon fiber prepreg coating	\	\	√	$\Delta R/R_0$ + 14%	[25]
3D textile composites	PVDF yarn	\	√	\	\	[42]
GFRP	MWCNT fabric coating	\	√	\	\	[43]
GFRP	MWCNT fabric coating	\	\	√	$\Delta R/R_0$-Δa model developed	[27]

SEM and Optical Microscope (OM) were used to analyze the fracture surface of the samples after model I tests. The control GFRP laminates [Figure 7A] display characteristic brittle fracture of epoxy (see white arrow) between adjacent fiber tows. The crack spreads preferentially along the fabric carbon fiber/epoxy matrix interface.

For GFRP embedded with a single PVDF film, part of the fibrous membrane remained on the fracture surface of the GFRP can be seen in Figure 7B. The green arrows in Figure 7C indicate there are traces of fibers pulled out from the remaining part of the nanofiber membrane. This suggests that the fibrous membrane was well infiltrated by the resin. The presence of the fibrous membrane altered the failure mode from adhesive to a mixed adhesive/cohesive mode within the interleave. This alteration increased the interlaminar toughness.

The fracture surface [Figure 7D and E] and cross section [Figure 7F] of the sandwich-structured PVDF sensor embedded GFRP were observed using SEM and OM, respectively. The crack growth within the middle layer PVDF can be seen (see red dotted lines in Figure 7F). The yellow arrows in Figure 7E and F show broken PVDF nanofibers. However, there are several non-infiltrated holes (see blue boxes in Figure 7E without resin bonding in the middle PVDF layer. While the crack propagates along the non-infiltrated holes, resulting in a decrease in the interlaminar toughness. The non-infiltrated holes may also lead to the slight decrease of mechanical properties. Due to the thickness of the sensor, the resin may not be able to completely infiltrate the entire sensor. Optimization of sensor infiltration can be enhanced through methods such as electrospinning microstructure design and drilling.

Table 2. Comparison of composite mechanical performance variation after sensor embedded in previous works[19]

Material	Sensors	Variation in mechanical properties			Reference
		Flexural strength & modulus	ILSS	Tensile strength & modulus	
GFRP	Pt-PVDF	+0.84% -1.12%	-0.73%	-0.34% -1.02%	[19]
GFRP	Copper-PVDF	-4.74% -1.32%	-8.15%	-0.58% -1.79%	[19]
GFRP	PVDF	-0.56% -4.51%	\	-5.67% -6.91%	[44]
CFRP	PVDF	\	-7.41%	+2.12% -2.11%	[45]
GFRP	Piezoelectric sensor	-8.00% 0%	\	\	[46]
CFRP	Lead zirconate titanate (PZT)	\	\	\ -20.98%	[47]
GFRP	PZT	\	-14.93%	-5.53% \	[48]
GFRP	Piezoelectric fiber composite sensors (PFCS)	\	-7.71%	-2.39% \	[48]
Composite sandwich structure	PFCS	-3.53%	-5.49%	-7.67% \	[17]
GFRP	CNT film	+4.72% +6.69%	-0.88%	-1.89% +4.74%	[49]
GFRP	Graphene fabric Coating	-37.00% -39.65%	\	-26.29% -8.48%	[50]

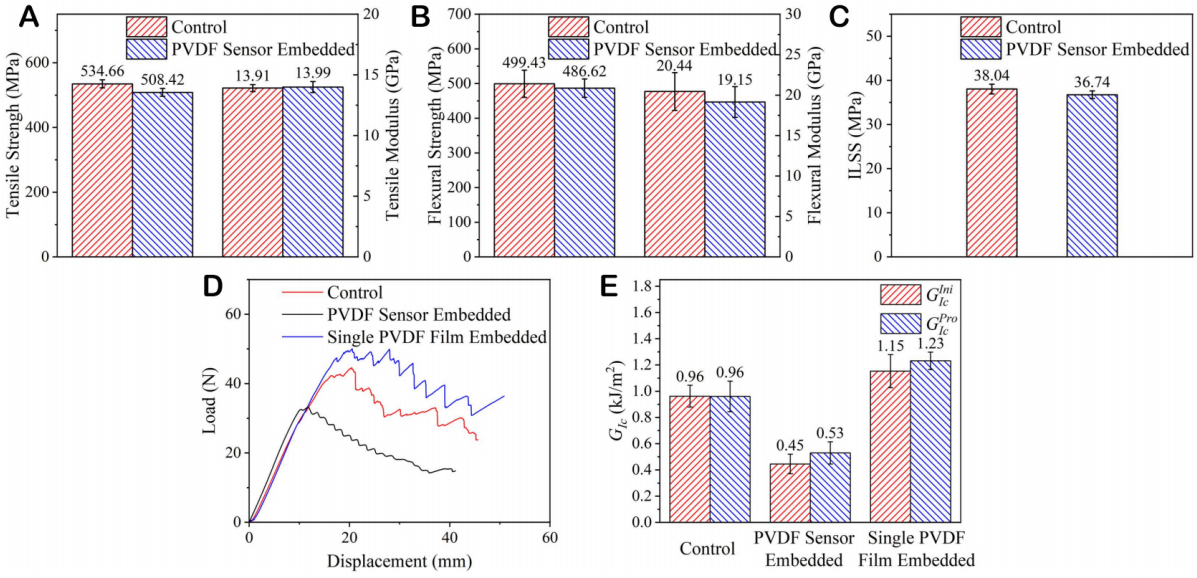

Figure 6. Comparison of GFRP with and without embedded PVDF sensor: (A) tensile strength and modulus; (B) flexural strength and modulus; (C) ILSS; GFRP control, GFRP embedded with single PVDF film and GFRP embedded with PVDF sensor (D) model I interlaminar fracture displacement-load curves; (E) G_{Ic}^{Ini} and G_{Ic}^{Pro}.

CONCLUSIONS

In this study, by utilizing the piezoelectric and dielectric characteristics of electrospun PVDF membranes, a sandwich-structured PVDF sensor is designed to realize the stress and interlaminar crack monitoring in GFRP structure. This sensor also meets the needs of embedded sensors without sacrificing mechanical

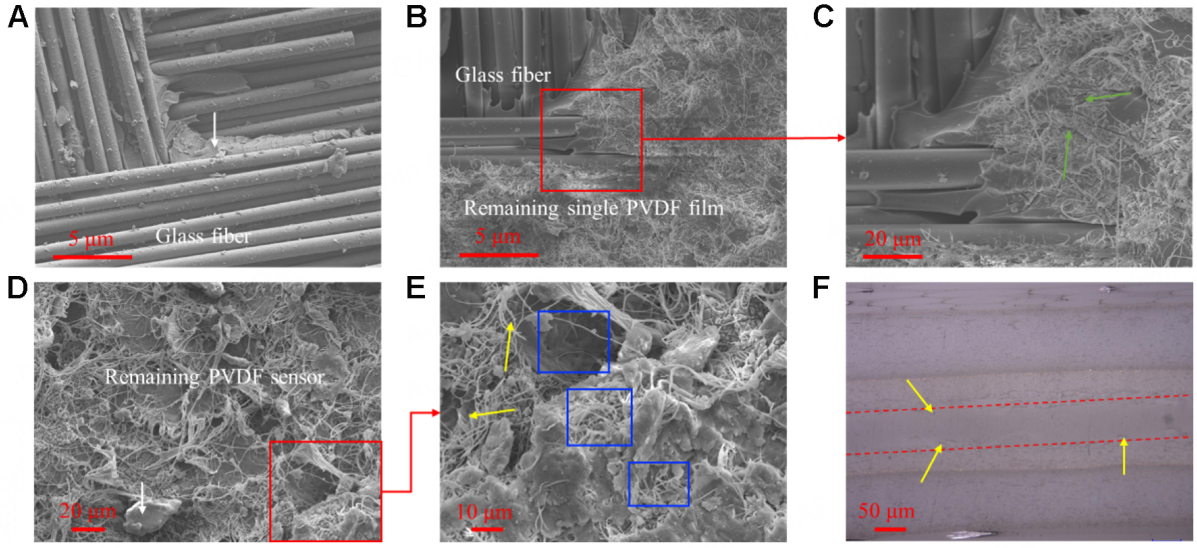

Figure 7. (A) SEM images of GFRP fracture surface; (B) SEM images of GFRP embedded single PVDF film fracture surface; (C) Infiltration state of GFRP embedded single PVDF film fracture surface; (D) SEM images of GFRP embedded sandwiched-structure PVDF sensor fracture surface; (E) Infiltration state of GFRP embedded sandwiched-structure PVDF sensor fracture surface; (F) OM images of GFRP embedded sandwiched-structure PVDF sensor cross section. Crack propagation direction was from left to right.

properties. By comparing with CNT films and copper electrodes, the Au-PVDF, which has a similar modulus to PVDF and does not cause conduction in the sensor, is employed as the sensor electrode.

In terms of sensing, the sensor's capacity to monitor the GFRP stress condition and fatigue failure was verified through dynamic three-point bending experiments. The Model I interlaminar fracture toughness test demonstrated the sensor's capacity to detect interlaminar cracks in GFRP by collecting capacitance data. Through a horizontal comparison with SHM for composites in other works, the innovation that the sensor in this work realizes the stress, failure and interlaminar crack monitoring of composite material components is illustrated.

In terms of mechanical performance, the sandwiched-structure PVDF sensor resulted in a slight decrease in basic mechanical properties (< -7%) but reduction in G_{Ic}^{Pro} (-44.79%), while single PVDF film leads to an increase (+28.13%). SEM and OM images reveal that the non-infiltrated area in the PVDF membrane ultimately led to a decrease in interlaminar toughness. Optimization of sensor infiltration can be enhanced through electrospinning microstructure design and drilling.

DECLARATIONS

Authors' contributions

Organized and literature review and draft the origin version: Lin H, Zhang F
Revised and manuscript: Peng Y, Ke X, Sai L, Wang F, Zhou H (Helezi Zhou), Zheng N, Huang Z
Conceived and supervised the project: Zhou H (Zhou Helezi), Huang Z, Zhou H (Huamin Zhou)

Availability of data and materials

According to reasonable requirements, all of the data examined in this research can be obtained from the correspondents.

Financial support and sponsorship
The authors would like to acknowledge the financial support from the National Natural Science Foundation of China (No. 52275336 and No. U20A20288).

Conflicts of interest
All authors declared that there are no conflicts of interest.

Ethical approval and consent to participate
Not applicable.

Consent for publication
Not applicable.

REFERENCES

1. Ghori SW, Siakeng R, Rasheed M, Saba N, Jawaid M. 2 - The role of advanced polymer materials in aerospace. In: Jawaid M, Thariq M, editors. Sustainable composites for aerospace applications. Elsevier; 2018, pp. 19-34. DOI
2. Sathishkumar T, Satheeshkumar S, Naveen J. Glass fiber-reinforced polymer composites - a review. *J Reinf Plast Compos* 2014;33:1258-75. DOI
3. Mouritz A, Gellert E, Burchill P, Challis K. Review of advanced composite structures for naval ships and submarines. *Compos Struct* 2001;53:21-42. DOI
4. Talreja R. Transverse cracking and stiffness reduction in composite laminates. *J Compos Mater* 1985;19:355-75. DOI
5. Li J, Zhang Z, Fu J, Liang Z, Ramakrishnan KR. Mechanical properties and structural health monitoring performance of carbon nanotube-modified FRP composites: a review. *Nanotechnol Rev* 2021;10:1438-68. DOI
6. Silversides I, Maslouhi A, LaPlante G. Acoustic emission monitoring of interlaminar delamination onset in carbon fibre composites. *Struct Heal Monit* 2013;12:126-40. DOI
7. Safri SNAB, Sultan MTH, Jawaid M. 7 - Damage analysis of glass fiber reinforced composites. In: Durability and life prediction in biocomposites, fibre-reinforced composites and hybrid composites. Elsevier; 2019. pp. 133-47. DOI
8. Wu S, Ladani RB, Ravindran AR, et al. Aligning carbon nanofibres in glass-fibre/epoxy composites to improve interlaminar toughness and crack-detection capability. *Compos Sci Technol* 2017;152:46-56. DOI
9. Senthil K, Arockiarajan A, Palaninathan R, Santhosh B, Usha KM. Defects in composite structures: its effects and prediction methods - a comprehensive review. *Compos Struct* 2013;106:139-49. DOI
10. Dong H, Liu H, Nishimura A, et al. Monitoring strain response of epoxy resin during curing and cooling using an embedded strain gauge. *Sensors* 2020;21:172. DOI PubMed PMC
11. Dawood TA, Shenoi RA, Sahin M. A procedure to embed fibre Bragg grating strain sensors into GFRP sandwich structures. *Compos Part A Appl Sci Manuf* 2007;38:217-26. DOI
12. Sante R. Fibre optic sensors for structural health monitoring of aircraft composite structures: recent advances and applications. *Sensors* 2015;15:18666-713. DOI PubMed PMC
13. Ramakrishnan M, Rajan G, Semenova Y, Farrell G. Overview of fiber optic sensor technologies for strain/temperature sensing applications in composite materials. *Sensors* 2016;16:99. DOI PubMed PMC
14. Tuloup C, Harizi W, Aboura Z, Meyer Y, Khellil K, Lachat R. On the use of in-situ piezoelectric sensors for the manufacturing and structural health monitoring of polymer-matrix composites: a literature review. *Compos Struct* 2019;215:127-49. DOI
15. Rocha H, Semprimoschnig C, Nunes JP. Sensors for process and structural health monitoring of aerospace composites: a review. *Eng Struct* 2021;237:112231. DOI
16. Su Y, Xu L, Zhou P, et al. In situ cure monitoring and in-service impact localization of FRPs using pre-implanted nanocomposite sensors. *Compos Part A Appl Sci Manuf* 2022;154:106799. DOI
17. Konka HP, Wahab MA, Lian K. On mechanical properties of composite sandwich structures with embedded piezoelectric fiber composite sensors. *J Eng Mater Technol* 2012;134:011010. DOI
18. Xiao Y, Qiao W, Fukuda H, Hatta H. The effect of embedded devices on structural integrity of composite laminates. *Compos Struct* 2016;153:21-9. DOI
19. Zhang F, Gong L, Wang F, et al. Embedded Pt-PVDF sensor without compromising mechanical properties of GFRP for on-line sensing. *Thin-Walled Struct* 2023;187:110702. DOI
20. Wang Q, Tian Y, Duongthipthewa A, et al. An embedded non-intrusive graphene/epoxy broadband nanocomposite sensor co-cured

with GFRP for in situ structural health monitoring. *Compos Sci Technol* 2023;236:109995. DOI
21. Yang G, Feng X, Wang W, OuYang Q, Liu L. Effective interlaminar reinforcing and delamination monitoring of carbon fibrous composites using a novel nano-carbon woven grid. *Compos Sci Technol* 2021;213:108959. DOI
22. Kravchenko OG, Pedrazzoli D, Kovtun D, Qian X, Manas-Zloczower I. Incorporation of plasma-functionalized carbon nanostructures in composite laminates for interlaminar reinforcement and delamination crack monitoring. *J Phys Chem Solids* 2018;112:163-70. DOI
23. Du X, Zhou H, Sun W, et al. Graphene/epoxy interleaves for delamination toughening and monitoring of crack damage in carbon fibre/epoxy composite laminates. *Compos Sci Technol* 2017;140:123-33. DOI
24. Zhang H, Liu Y, Bilotti E, Peijs T. In-situ monitoring of interlaminar shear damage in carbon fibre composites. *Adv Compos Lett* 2015;24:096369351502400. DOI
25. Li M, Li S, Xiao J, Fu Y, Zhu W, Ke Y. An integrated nanofiller spray and nanosecond pulse electrically-assisted method for synergistically interlaminar toughening and in-situ damage monitoring of CFRP composites. *Compos Part B Eng* 2024;275:111355. DOI
26. Liu H, Qu P, Yu S, Xu Y, Jia Y. Low-cost carbon black-loaded functional films for interlaminar toughening and in-situ delamination monitoring of carbon fiber/epoxy composites. *J Appl Polym Sci* 2022;139:52170. DOI
27. Wan Y, Yang H, Tian Z, et al. Mode I interlaminar crack length prediction by the resistance signal of the integrated MWCNT sensor in WGF/epoxy composites during DCB test. *J Mater Res Technol* 2020;9:5922-33. DOI
28. Kravchenko OG, Pedrazzoli D, Bonab VS, Manas-Zloczower I. Conductive interlaminar interfaces for structural health monitoring in composite laminates under fatigue loading. *Mater Des* 2018;160:1217-25. DOI
29. Liu Y, Luo H, Xie H, et al. Trilayer PVDF nanocomposites with significantly enhanced energy density and energy efficiency using $0.55Bi_{0.5}Na_{0.5}TiO_3$-$0.45(Sr_{0.7}Bi_{0.2})TiO_3$ nanofibers. *Microstructures* 2023;3:2023008. DOI
30. Yang W, Li N, Zhao S, et al. A breathable and screen-printed pressure sensor based on nanofiber membranes for electronic skins. *Adv Mater Technol* 2018;3:1700241. DOI
31. Rani SD, Ramachandran R, Sheet S, et al. $NiMoO_4$ nanoparticles decorated carbon nanofiber membranes for the flexible and high performance glucose sensors. *Sensors Actuat B Chem* 2020;312:127886. DOI
32. Lin L, Park S, Kim Y, et al. Wearable and stretchable conductive polymer composites for strain sensors: how to design a superior one? *Nano Mater Sci* 2023;5:392-403. DOI
33. Cao T, Shi XL, Zou J, Chen ZG. Advances in conducting polymer-based thermoelectric materials and devices. *Microstructures* 2021;1:2021007. DOI
34. Ding B, Wang M, Yu J, Sun G. Gas sensors based on electrospun nanofibers. *Sensors* 2009;9:1609-24. DOI PubMed PMC
35. Zheng N, Song Y, Lan M, Dong X, Zhou H, Gao J. Improved interlaminar property of carbon fiber/epoxy composites with polyurethane/RGO core-shell structure fibrous mat. *Compos Commun* 2023;44:101748. DOI
36. Cheng WH, Wu PL, Huang HH. Electrospun polyvinylidene fluoride piezoelectric fiber glass/carbon hybrid self-sensing composites for structural health monitoring. *Sensors* 2023;23:3813. DOI PubMed PMC
37. Leung CM, Chen X, Wang T, et al. Enhanced electromechanical response in PVDF-BNBT composite nanofibers for flexible sensor applications. *Materials* 2022;15:1769. DOI PubMed PMC
38. Chen X, Cheng S, Wen K, et al. In-situ damage self-monitoring of fiber-reinforced composite by integrating self-powered ZnO nanowires decorated carbon fabric. *Compos Part B Eng* 2023;248:110368. DOI
39. Dubois D, Esteva F, Garcia P, Godo L, De Màntaras RL, Prade H. Case-based reasoning: a fuzzy approach. In: Ralescu AL, Shanahan JG, editors. Fuzzy logic in artificial intelligence. Berlin: Springer; 1999. pp. 79-90. DOI
40. Chen X, Cheng S, Wang S, et al. Embedding stretchable, mesh-structured piezoresistive sensor for in-situ damage detection of glass fiber-reinforced composite. *Compos Sci Technol* 2023;233:109926. DOI
41. Sánchez-Romate X, González C, Jiménez-Suárez A, Prolongo SG. Novel approach for damage detection in multiscale CNT-reinforced composites via wireless Joule heating monitoring. *Compos Sci Technol* 2022;227:109614. DOI
42. Kang J, Liu T, Lu Y, et al. Polyvinylidene fluoride piezoelectric yarn for real-time damage monitoring of advanced 3D textile composites. *Compos Part B Eng* 2022;245:110229. DOI
43. Rubio-González C, de Urquijo-Ventura MDP, Rodríguez-González JA. Damage progression monitoring using self-sensing capability and acoustic emission on glass fiber / epoxy composites and damage classification through principal component analysis. *Compos Part B Eng* 2023;254:110608. DOI
44. Rosa IM, Sarasini F. Use of PVDF as acoustic emission sensor for in situ monitoring of mechanical behaviour of glass/epoxy laminates. *Polym Test* 2010;29:749-58. DOI
45. Bae JH, Lee SW, Chang SH. Characterization of low-velocity impact-induced damages in carbon/epoxy composite laminates using a poly(vinylidene fluoride-trifluoroethylene) film sensor. *Compos Part B Eng* 2018;135:189-200. DOI
46. Masmoudi S, El Mahi A, Turki S. Fatigue behaviour and structural health monitoring by acoustic emission of E-glass/epoxy laminates with piezoelectric implant. *Appl Acoust* 2016;108:50-8. DOI
47. Feng T, Aliabadi MHF. Structural integrity assessment of composites plates with embedded PZT transducers for structural health monitoring. *Materials* 2021;14:6148. DOI PubMed PMC
48. Konka HP, Wahab MA, Lian K. The effects of embedded piezoelectric fiber composite sensors on the structural integrity of glass-fiber-epoxy composite laminate. *Smart Mater Struct* 2012;21:015016. DOI
49. Buggisch C, Gibhardt D, Felmet N, Tetzner Y, Fiedler B. Strain sensing in GFRP via fully integrated carbon nanotube epoxy film

sensors. *Compos Part C Open Access* 2021;6:100191. DOI

50. Reghat M, Mirabedini A, Tan AM, et al. Graphene as a piezo-resistive coating to enable strain monitoring in glass fiber composites. *Compos Sci Technol* 2021;211:108842. DOI
51. Han S, Li Q, Cui Z, et al. Non-destructive testing and structural health monitoring technologies for carbon fiber reinforced polymers: a review. *Nondestruct Test Eval* 2024;39:725-61. DOI